J|A|C|S
ARTICLES
Published on Web 01/22/2002

Hierarchical Self-Assembly of Amphiphilic Metallohosts To Give Discrete Nanostructures

Johannes A. A. W. Elemans,* Alan E. Rowan, and Roeland J. M. Nolte

Contribution from the Department of Organic Chemistry, NSR Center, University of Nijmegen, Toernooiveld, 6525 ED Nijmegen, The Netherlands

Received August 27, 2001

Abstract: The synthesis and aggregation behavior of a new class of rigid metallohosts is described. The molecules consist of a ruthenium−bipyridine complex functionalized with a glycoluril-based receptor cavity. By specific molecular recognition processes in water, the metallohosts self-assemble to form large arrays of molecules. Depending on the size of the cavity side walls of the host, these arrays can grow in a hierarchical process into discrete rectangular and cigarlike aggregates of nanometer size, which can be visualized by electron microscopy.

Introduction

The ability to have control over processes leading to the self-assembly of molecules and the formation of nanosized structures of well-defined size and shape is one of the challenges facing modern chemistry.[1,2] In nature, self-assembly involves the noncovalent organization of molecules containing specific information needed for intermolecular recognition processes to occur, e.g., hydrogen bonding, π-stacking, van der Waals, and electrostatic interactions.[3] By using complementarity of shape as a tool and by applying directed intermolecular forces, in combination with entropy-driven processes, nature is capable of assembling building blocks into nanosized objects of precisely determined shape, structure, and function.

During the past decade, many examples have been published of synthetic approaches that result in the formation of predesigned supramolecular architectures. A more recent development is the incorporation of metals into these architectures,[4] which can, in principle, give functionality. The ordering of (transition) metals in well-defined positions and at mutually fixed distances may eventually lead to new applications in materials science and catalysis.[5] Most of the metalloassemblies known to date can be divided into two categories: (i) well-defined multimetal complexes consisting of a relatively small number (<50) of constituting building blocks that are self-assembled in solution[6] and (ii) infinite solid-state metalloarrays (metallocrystals).[7] The first class of assemblies, which are commonly referred to as coordination-directed self-assemblies,[8] comprises a wide range of systems, e.g., metal-containing molecular grids,[9] metallacycli,[10] helicates,[11,12] metallodendrimers,[13] metallocages and metallocapsules,[14] and metallotubes.[15] The properties that these structures have in common are their finite size but also their close to nanoscopic dimension. Only a limited number of components are usually assembled, the largest discrete metalloassembly to date being a metallododecahedron that is constructed from 50 components and has a diameter of approximately 8 nm.[16] The limitation in the construction of larger architectures via this approach lies mainly in the thermodynamics of the assembly process, in particular the relative stabilities of the intermediates and the final product. When such a product is

* To whom correspondence should be addressed: e-mail jelemans@sci.kun.nl/rowan@sci.kun.nl.

(1) Whitesides, G. M.; Mathias, J. P.; Seto, C. T. *Science* **1991**, *254*, 1312.
(2) (a) Lbotak, P.; Shinkai, S. *Tetrahedron Lett.* **1995**, *36*, 4829. (b) Philp, D.; Stoddart, J. F. *Angew. Chem., Int. Ed. Engl.* **1996**, *35*, 1155. (c) Gillard, R. E.; Raymo, F. M.; Stoddart, J. F. *Chem. Eur. J.* **1997**, *3*, 1933. (d) Chemseddine, A.; Moritz, T. *Eur. J. Inorg. Chem*. **1999**, 235. (e) Rebek, J., Jr. *Acc. Chem. Res.* **1999**, *32*, 278. Aizenberg, J.; Black, A. J.; Whitesides, G. M. *Nature* **1999**, *398*, 495. (f) Ozin, G. A. *Can. J. Chem.* **1999**, *77*, 2001. (g) Li, M.; Schnablegger, H.; Mann, S. *Nature* **1999**, *402*, 393. (h) Orr, G. W.; Barbour, L. J.; Atwood, J. L. *Science* **1999**, *285*, 1049.
(3) Lehn, J.-M. In *Supramolecular Chemistry*; VCH: Weinheim, Germany, 1995.
(4) Reviews: (a) Baxter, P. N. W. In *Comprehensive Supramolecular Chemistry*; Atwood, J. L., Davies, J. E. D., MacNicol, D. D., Vögtle, F., Reinhoudt, D. N., Lehn, J.-M., Eds.; Elsevier Science Ltd., Pergamon: Elmsford, 1996; Vol. 9, p 165. (b) Fujita, M. *Ibid*., p 253. (c) Constable, E. C. *Ibid*., p 213.
(5) Service, R. F. *Science* **1994**, *265*, 316.
(6) Reviews: (a) Fujita, M. *Chem. Soc. Rev.* **1998**, *27*, 417. (b) Caulder, D. L.; Raymond, K. N. *Acc. Chem. Res.* **1999**, *32*, 975.
(7) Review: Batten, S. R.; Robson, R. *Angew. Chem., Int. Ed. Engl.* **1998**, *37*, 1461.
(8) Levin, M. D.; Stang, P. J. *J. Am. Chem. Soc.* **2000**, *122*, 7428.
(9) Baxter, P. N. W.; Lehn, J.-M.; Kneisel, B.; Fenske, D. *Angew. Chem., Int. Ed. Engl.* **1997**, *36*, 1978.
(10) Reviews: (a) Stang, P. J.; Olenyuk, B. *Acc. Chem. Res.* **1997**, *30*, 502. (b) Leininger, S.; Olenyuk, B.; Stang, P. J. *Chem. Rev.* **2000**, *100*, 853.
(11) (a) Hasenknopf, B.; Lehn, J.-M.; Boumediene, N.; Dupont-Geravis, A.; van Dorsselaer, A.; Kneisel, B.; Fenske, D. *J. Am. Chem. Soc.* **1997**, *119*, 10956. (b) Withersby, M. A.; Blake, A. J.; Champness, N. R.; Hubberstey, P.; Li, W.-S.; Schröder, M. *Angew. Chem., Int. Ed. Engl.* **1997**, *36*, 2327. (c) Kaes, C.; Hosseini, M. W.; Rickard, C. E. F.; Skelton, B. W.; White, A. H. *Angew. Chem., Int. Ed. Engl.* **1998**, *37*, 920.
(12) See for a review about helical programming: Rowan, A. E.; Nolte, R. J. M. *Angew. Chem., Int. Ed. Engl.* **1998**, *37*, 63.
(13) (a) Huck, W. T. S.; Prins, L. J.; Fokkens, R. H.; Nibbering, N. M. M.; van Veggel, F. C. J. M.; Reinhoudt, D. N. *J. Am. Chem. Soc.* **1998**, *120*, 6240. (b) Newkome, G. R.; He, E. F.; Moorefield, C. N. *Chem. Rev.* **1999**, *99*, 1689.
(14) (a) Jacopozzi, P.; Dalcanale, E. *Angew. Chem., Int. Ed. Engl.* **1997**, *36*, 613. (b) Fujita, M.; Yu, S.-Y.; Kusukawa, T.; Funaki, H.; Ogura, K.; Yamaguchi, K. *Angew. Chem., Int. Ed. Engl.* **1998**, *37*, 2082. (c) Fox, O. D.; Dalley, N. K.; Harrison, R. G. *J. Am. Chem. Soc.* **1998**, *120*, 7111. (d) Kusukawa, T.; Fujita, M. *J. Am. Chem. Soc.* **1999**, *121*, 1397. (e) Hiraoka, S.; Fujita, M. *J. Am. Chem. Soc.* **1999**, *121*, 10239.
(15) Aoyagi, M.; Biradha, K.; Fujita, M. *J. Am. Chem. Soc.* **1999**, *121*, 7457.
(16) Olenyuk, B.; Levin, M. D.; Whiteford, J. A.; Shield, J.; Stang, P. J. *J. Am. Chem. Soc.* **1999**, *121*, 10434.

10.1021/ja012061i CCC: $22.00

Chart 1

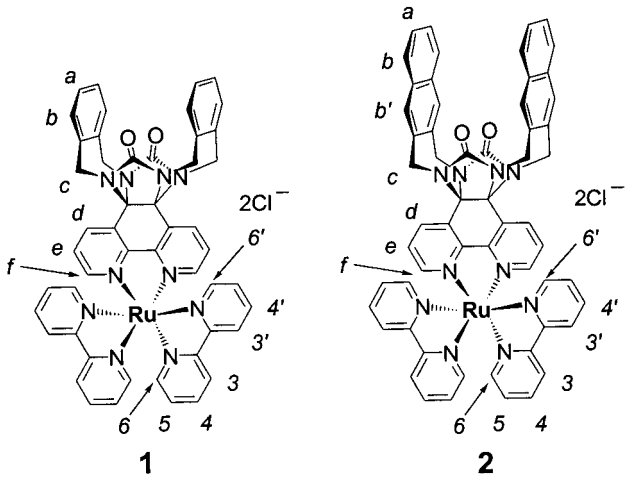

built up from an increasing number of components, nondiscrete structures with different geometries may also be formed since they have similar energies as the desired, discrete product. Approaches to bridge the gap between the small, nanoscopic assemblies mentioned above and the extended solid-state structures have been reported only recently. Metallosuperstructures of mesoscopic scale have been constructed by combining metal ions with self-organizing organic counterions.[17,18] A different approach involved the templated deposition of charged coordination complexes around oppositely charged nanoparticles, resulting in the formation of discrete and well-defined objects of about 75 nm size.[19]

This paper deals with the construction of discrete nanosized objects from metal complexes containing a ligand with molecular recognition properties. We describe the synthesis of compounds **1** and **2** (Chart 1), which are water-soluble $[Ru(bipy)_3]^{2+}$ complexes in which one of the bipyridine ligands is functionalized with a molecular clip receptor.[20] Furthermore, the self-assembly of these metallohosts into discrete micrometer-sized aggregates in water is reported, as well as the manipulation of these aggregates by varying the temperature.[21]

Results and Discussion

Synthesis and Characterization. The synthesis of **1** and **2** (Chart 1) started with the acid-catalyzed condensation of urea and 5,6-dihydro[1,10]phenanthroline-5,6-dione[22] in toluene to give bipyridine−glycoluril compound **3** as a solid material in 86% yield (Scheme 1). Alkylation of **3** with 1,2-bis(bromomethyl)benzene in dimethyl sulfoxide (DMSO), with KOH as a base, gave **4** in a yield of 31%, after recrystallization from methanol. Similar alkylation of **3** with 2,3-bis(bromomethyl)-naphthalene afforded **5** in a yield of 26%. In the crystal structure that was resolved for **4**[21] (Figure 1), a severe twist in the glycoluril framework is visible, which is most clearly expressed

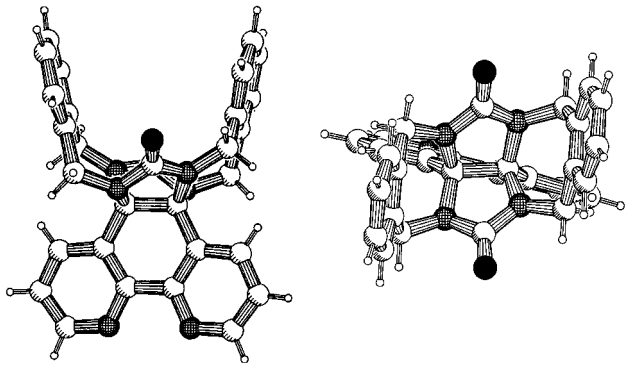

Figure 1. X-ray structure of **4** (front and top view).

Scheme 1

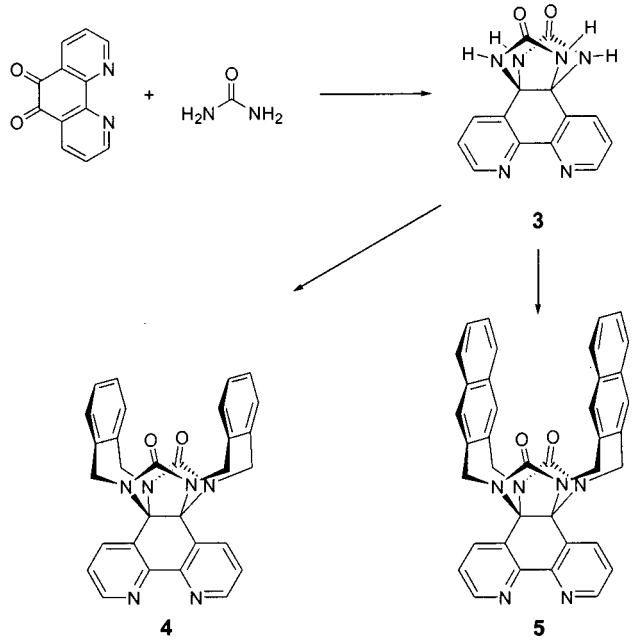

in the twisting of the cavity side walls. Furthermore, the large steric interaction between the 5,5′-bipyridine and methylene protons causes the cavity to be squeezed and narrowed when compared to cavities of receptors based on diphenylglycoluril. This is reflected in a relatively small distance between the centers of the aromatic side walls of **4** (6.18 Å).

Receptor molecules **4** and **5** were then complexed with $[Ru(bipy)_2]Cl_2 \cdot 2H_2O$[23] in DMF to give metallohosts **1** and **2** (Chart 1) in 55% and 87% yields, respectively. The compounds had an orange-red color, which is characteristic for $Ru(bipy)_3$ derivatives. Due to the chiral nature of the octahedral ruthenium center, **1** and **2** are racemic mixtures of Λ and Δ enantiomers, and as a result they exhibit complicated NMR spectra. With the help of correlated spectroscopy (COSY) and two-dimensional nuclear Overhauser effect spectroscopy (2D NOESY) techniques (500 MHz), however, the resonances of all the protons of **1** and **2** in D_2O solution could be assigned.

NMR Dilution Studies. It was expected that the hydrophobic receptor cavities of **1** and **2** would self-associate in water, since this property was previously observed for other water-soluble cavity molecules based on glycoluril.[24] The ^1H NMR spectra

(17) Ding, J. H.; Gin, D. L. *Chem. Mater.* **2000**, *12*, 22.
(18) (a) Kimizuka, N.; Lee, S. H.; Kunitake, T. *Angew. Chem., Int. Ed. Engl.* **2000**, *39*, 389. (b) Kimizuka, N.; Oda, N.; Kunitake, T. *Inorg. Chem.* **2000**, *39*, 2684.
(19) Kurth, D. G.; Caruso, F.; Schüler, C. *Chem. Commun.* **1999**, 1579.
(20) For a review about molecular clips see: Rowan, A. E.; Elemans, J. A. A. W.; Nolte, R. J. M. *Acc. Chem. Res.* **1999**, *32*, 995.
(21) Part of this work has been published as a preliminary communication: Elemans, J. A. A. W.; de Gelder, R.; Rowan, A. E.; Nolte, R. J. M. *Chem. Commun.* **1998**, 1553.
(22) Yamada, M.; Tanaka, Y.; Yoshimoto, Y.; Kuroda, S.; Shimao, I. *Bull. Chem. Soc. Jpn.* **1992**, *65*, 1006.
(23) Sullivan, B. P.; Meyer, T. J. *Inorg. Chem.* **1978**, *17*, 3334.
(24) (a) Reek, J. N. H.; Kros, A.; Nolte, R. J. M. *Chem. Commun.* **1996**, 245. (b) Isaacs, L.; Witt, L. D.; Fettinger, J. C. *Chem. Commun.* **1999**, 2549.

Table 1. Self-Association Constants (K_{Self}, M^{-1}) and CIS Values (ppm) for **1** and **2** in D_2O at 298 K, Calculated with Several Shifting Protons as a Probe

	metallohost			
	1		**2**	
proton[a]	K_{self}[b] (M^{-1})	CIS[b] (ppm)	K_{self}[c] (M^{-1})	CIS[b] (ppm)
H_a	58	−0.85	21 000	−2.07
H_b	55	−0.45	*d*	*d*
$H_{b'}$			*d*	*d*
H_4	52	−1.41	2900	−0.33
H_5	47	−0.58	2300	−0.27

[a] For proton numbering see Chart 1. [b] Estimated error approximately 10%. [c] Estimated error approximately 40%. [d] No reliable value could be obtained due to overlap and broadening of the signals.

of **1** in D_2O displayed sharp resonances up to relatively high (>30 mM) concentrations, which enabled a reliable and detailed study of the self-association behavior of this molecule. Several proton resonances in the spectra of **1** were very sensitive to changes in concentration and temperature. Upon dilution, the resonances of the side-wall protons H_a and H_b and the bipyridine protons H_4 and H_5 (see Chart 1) exhibited large downfield shifts, whereas the resonances of all the other protons of **1** displayed only relatively small up- or downfield shifts (<0.1 ppm). Upon warming a solution of **1**, shifts similar to observed upon dilution were visible. An NMR dilution titration of **1** in D_2O, with samples that varied in concentration from 0.5 to 10 mM, was carried out, and the chemical shifts of the resonances that displayed the largest shifts (H_a, H_b, H_4, and H_5) were plotted versus concentration. The resulting titration curves could all be fitted to an equation defining a 1:1 self-association process. The self-association constant K_{self} between two molecules of **1** was determined to be 53 ± 6 M^{-1} (Table 1). To obtain additional information about the exact geometry of the molecules of **1** in the dimer, 2D NOESY spectra were recorded at different concentrations of the compound in D_2O. At a concentration of 1 mM, only cross-peaks were observed resulting from nearest-neighbor proton contacts, indicating the presence of (predominantly) non-self-associated **1** in solution. In the 2D NOESY spectrum of a 30 mM solution of **1** in D_2O, in addition to cross-peaks that can be expected because of nearest-neighbor contacts, now cross-peaks were observed between the signals of side-wall protons H_a/H_b and the set of bipyridine protons H_4/H_5,H_6,$H_{6'}$ and between the signals of H_a/H_b and $H_d/H_e/H_f$ (Chart 1). These cross-peaks can only be the result of *inter*molecular close contacts, which, at the used concentration, points to dimerization or aggregation of **1**. Combining the results obtained from the NOESY experiment with the complexation-induced shift (CIS) values calculated from the dilution titration (Table 1), a well-defined head-to-tail self-assembly geometry of **1** in water can be proposed. In this assembly the sterically least hindered side of one of the bipyridine ligands is clipped between the cavity side walls of its neighbor. By use of the observed intermolecular nuclear Overhauser effect (nOe) contacts in combination with molecular modeling, the geometry of this self-associated head-to-tail dimer was calculated (Figure 2a,b). In the mode of assembly, a tight fit exists between two adjacent molecules, which combines maximal cavity-filling with minimal exposure of the hydrophobic aromatic surfaces to water. In the dimer, favorable offset $\pi-\pi$ interactions[25] are present between the two side walls and the clamped bipyridine ligand and between one of the side walls and the other bipyridine ligand,

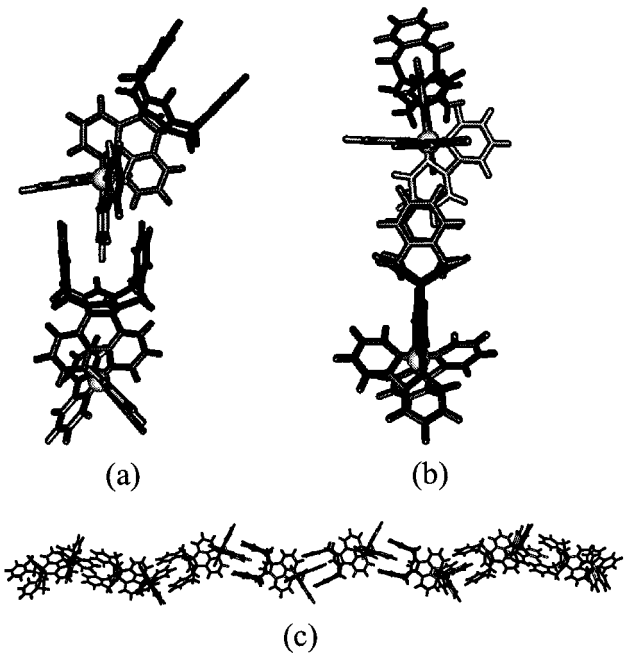

Figure 2. Computer-modeled structures of the modes of self-association of **1** in water, calculated with the CIS values from the NMR dilution titrations and the observed intermolecular nOe contacts. (a, b) Front and side view of the head-to-tail self-association of two molecules of **1**. (c) Infinite array of molecules of **1**, which is a result of a repeated head-to-tail self-association process in water.

which is positioned in an edge-to-face geometry on top of it. Molecular modeling clearly indicated that simultaneous binding of *both* bipyridine ligands of a molecule of **1** to *two* neighboring molecules is not possible, due to the occurrence of considerable steric hindering between the molecules in such a 2:1 complex.[26] It is, however, expected that self-association of **1** in water is not restricted to the formation of dimers only, since one of the dimeric partners has a free cavity that is available for complexing another molecule of **1**. The binding in the cavity and the complexation of the bipyridine ligands within the cavity of a neighboring molecule of **1** are thought to be independent processes. Depending on the concentration, long arrays of **1** can be formed in solution (Figure 2c) and the calculated K_{self} clearly is an apparent self-association constant.

Upon dilution of metallohost **2** in D_2O, the resonances of the side-wall protons H_a, H_b and $H_{b'}$ and of the bipyridine protons H_4 and H_5 (see Chart 1) exhibited strong downfield shifts, in particular the signal of the top side-wall protons (H_a), suggesting that **2** self-associates in a head-to-tail geometry similar to that of **1**. The signals of **2** were significantly broadened even at low concentration, and at concentrations above 2 mM the solution gradually turned into a turbid dispersion. An NMR dilution titration, carried out on samples varying in concentration between 0.1 and 2 mM, indicated a self-association that was significantly stronger than that observed for **1** (Table 1). Remarkably, when K_{self} was calculated with the side-wall proton signals of **2** as probes ($K_{self} = 21\,000$ M^{-1}), the value appeared

(25) (a) Hunter, C. A.; Sanders, J. K. M. *J. Am. Chem. Soc.* **1990**, *112*, 5525. (b) Reek, J. N. H.; Priem, A. H.; Engelkamp, H.; Rowan, A. E.; Elemans, J. A. A. W.; Nolte, R. J. M. *J. Am. Chem. Soc.* **1997**, *119*, 9956. (c) Breault, G. A.; Hunter, C. A.; Mayers, P. C. *J. Am. Chem. Soc.* **1998**, *120*, 3402. (d) Whitten, D. G.; Chen, L.; Geiger, H. C.; Perlstein, J.; Song, X. *J. Phys. Chem. B.* **1998**, *102*, 10098.

(26) A 2:1 complex was excluded since the data points could not be fitted to an equation defining such a 2:1 complex.

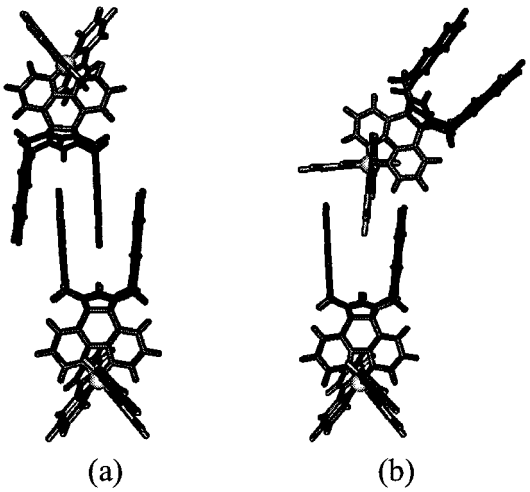

Figure 3. Computer-modeled structures of two self-associated dimers of **2** in water. (a) Head-to-head dimer. (b) Head-to-tail dimer.

Table 2. Photophysical Properties of $[Ru(bipy)_3]Cl_2$, **1**, and **2** (all 10^{-5} M) in Water at 298 K

complex	λ_{max}(MLCT), nm	λ_{em}(MLCT), nm	emission intensity, au
$[Ru(bipy)_3]Cl_2$	453	596	295
1	447	628	70
2	450	625	35

to be substantially different from the value that was calculated with the bipyridine protons as the probe ($K_{self} \sim 2500$ M^{-1}). The fact that two different K_{self} values were measured for the different sets of protons of **2** suggests that, apart from the calculated head-to-tail geometry (Figure 3b), a second self-association geometry occurs, viz., a head-to-head one that involves a strong self-association of the large naphthalene-walled cavities in a head-to-head geometry (Figure 3a). The latter process is dominated by hydrophobic interactions: **2** possesses a much larger hydrophobic cavity than **1** and hence is expected to form much stronger head-to-head dimers. This phenomenon is further reflected in the very large CIS value measured for the H_a protons of **2** (Table 1).

UV−Vis and Fluorescence Studies. Ruthenium−bipyridine complexes are well-known for their rich photophysical properties.[27] In Table 2 the spectral data for complexes **1** and **2** in water, and for comparison those of $[Ru(bipy)_3]Cl_2$, are listed. Compared to the absorption spectrum of $[Ru(bipy)_3]Cl_2$, the metal-to-ligand charge transfer (MLCT) bands (between 400 and 500 nm) of **1** and **2** are somewhat broader, which is probably caused by the fact that one of the bipyridine ligands in these compounds is substituted. The emission maxima of the metallohosts recorded upon irradiation of the MLCT band are clearly red-shifted with respect to the emission maximum of $[Ru(bipy)_3]Cl_2$. This is a commonly observed phenomenon since the wavelengths of the emission maxima are known to be more sensitive to the substitution pattern of the bipyridine ligands than the wavelengths of the absorption maxima.[28]

To investigate the influence of the concentration on the absorption and emission spectra, solutions of the ruthenium complexes in water varying in concentration from 10^{-8} to 10^{-4} mM were prepared and measured. These variations in concentration appeared to have no influence on the absorption spectra, indicating that no excitonic interactions between the molecules were present. At all concentrations, the emission of **1** and **2** was significantly less intense when compared to the emission of $[Ru(bipy)_3]Cl_2$. Apparently, the self-quenching of the metallohosts is stronger than the self-quenching of $[Ru(bipy)_3]Cl_2$, which can be attributed to aggregation effects of the former compounds. Further support for this comes from the fact that the emissions of **1** and **2** increased and became almost equal to the emission of $[Ru(bipy)_3]Cl_2$ when a small quantity (5%) of acetone, a solvent that is known to cause dissociation of related self-assembled structures in water,[24] was added to the solutions of the metallohosts.

Electron Microscopy Studies. To investigate whether the self-association of the metallohosts resulted in the formation of large aggregates, samples of **1** and **2** in water were investigated by transmission electron microscopy (TEM).[29] Solutions of **1** in water remained clear up to relatively high concentrations (>30 mM).[30] Samples of these solutions were deposited on a Formvar-coated copper grid and studied with TEM. Rather undefined, scroll-like assemblies were observed with lengths up to 10 μm and a typical width of approximately 100 nm (Figure 4a).

When the concentration of compound **2** in water was increased to approximately 2 mM, the solution transformed into a turbid dispersion. This turbidity remained for days without any precipitation occurring. This suggests that relatively large aggregates are present. Indeed, when samples of a dispersion [0.5% (w/v) **2**] were studied by TEM, discrete rectangular aggregates were observed (Figure 4b,c), which were very monodisperse in shape and size (typical dimensions 350 × 150 nm). The grids were subsequently shadowed with platinum under a 45° angle, which allowed the determination of the height of the rectangles. They appeared to be also relatively monodisperse in height, viz., 75 ± 10 nm.

Somewhat surprisingly, occasionally instead of rectangular structures cigarlike aggregates were observed (Figure 5a), which were an order of magnitude larger (typical dimensions 4000 × 350 nm) than the rectangular ones. Analysis of these cigars revealed that they were also highly monodisperse in both shape and size (aspect ratio length:width = 11 ± 2). Some of the cigars displayed transverse cracks (Figure 5b), which surprisingly slowly healed when the structure was held for a couple of seconds in the electron beam of the microscope. A closer look at the cigars at higher magnification revealed that they were built up from smaller subunits (Figure 5c,d). These subunits appeared to have dimensions that were remarkably similar to the length and height of the rectangular aggregates (300−400 × 75 nm). We propose that the cigarlike aggregate is a higher-order assembly, which is constructed from a limited number (40−60) of rectangular aggregates. To date, however, we have not yet found the precise conditions for this hierarchical growth process. Variations in the concentration of **2** (0.1−2.0% w/v) and a systematic pretreatment of the

(27) Review: Juris, A.; Balzani, V.; Barigelletti, F.; Campagna, S.; Belser, P.; von Zelewsky, A. *Coord. Chem. Rev.* **1988**, *84*, 85.
(28) Issberner, J.; Vögtle, F.; De Cola, L.; Balzani, V. *Chem. Eur. J.* **1997**, *3*, 706.
(29) Initially, these studies were carried out without applying shadowing or staining techniques, implying that any observed contrast is the result of the ruthenium centers in the molecules.
(30) At higher concentrations the compounds started to precipitate and no dispersions were obtained as in the case of **2**.

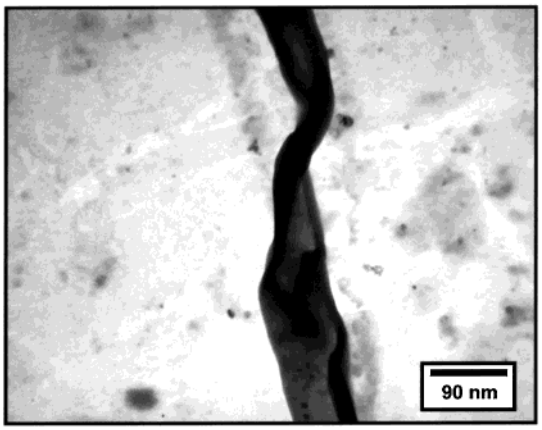

(a)

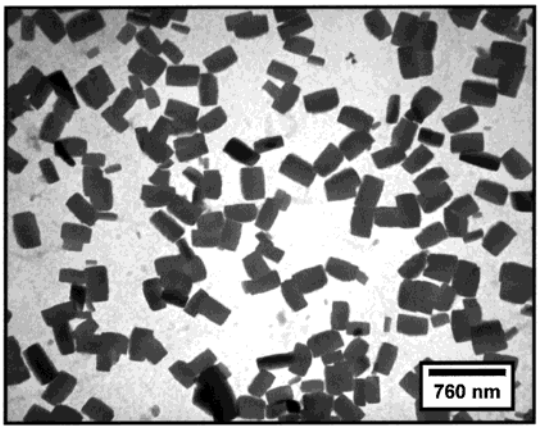

(b)

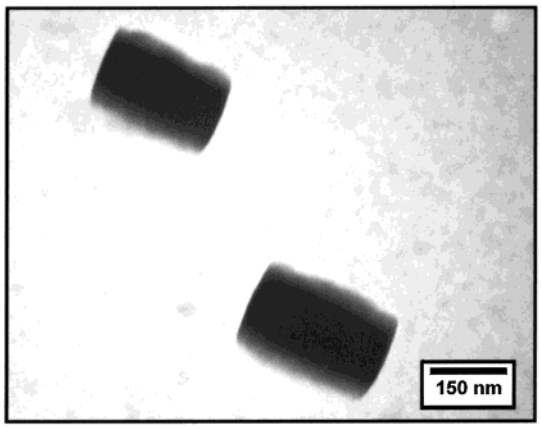

(c)

Figure 4. (a) TEM image of scroll-like aggregates as typically formed by **1**. (b, c) TEM images of the rectangular aggregates formed by **2**. Samples are not shadowed or stained.

dispersions (heating, cooling, ultrasonication, or combinations thereof) did not lead to increased amounts of the cigarlike superstructures.

To study the effect of the temperature on the aggregate morphology, 0.5% (w/v) dispersions of **2** in water were prepared at 20, 50, and 70 °C, respectively. Samples of these dispersions were preincubated for 30 min, deposited on grids, and studied with the help of TEM. In all cases, the observed aggregates were well-defined and rectangular in shape. The observed size dispersity of the structures appeared, however, to be dependent on the temperature. For each sample, the lengths and widths of a large number of aggregates (approximately 300−400) were measured and their size distribution was plotted (Figure 6). From these distributions it can be seen that at higher temperatures the rectangles are far more monodisperse in size than at lower temperature. In addition, the aggregate size tends to become smaller at higher temperatures.[31]

Aggregate Growth Model. The scroll-like aggregates that are formed by **1** are rather undefined when compared to the rectangular and cigarlike structures formed by **2**. The observation that **2** assembles into a better defined supramolecular structure than **1** is attributed to the much stronger self-association of the former molecule. The naphthalene side walls in **2** are large hydrophobic surfaces that can significantly enhance the interaction between neighboring stacked molecules. This may result in a more compact and more well-defined structure at the mesoscopic level.

On the basis of the ^{1}H NMR dilution experiments in water and the electron microscopy studies, we propose that the rectangular aggregates grow as outlined in Figure 7. The growth starts with the formation of a head-to-head dimer, which is the unit corresponding to the strongest interactions between two molecules of **2**. We presume that the dimer then acts as a nucleation point for further growth in two dimensions: as a result of the strong, hydrophobic interactions between the large naphthalene surfaces, the dimers of **2** stack to form an extended bilayerlike array, which grows away in two directions from the central dimer. In this bilayer array, the so-called dimeric seed, all the hydrophilic ruthenium−bipyridine units are supposed to be directed toward the aqueous phase. An additional process probably takes place simultaneously, in which monomers of **2** attach themselves in a head-to-tail fashion to the bipyridine units of the above-mentioned bilayer array of dimers, eventually resulting in the formation of a two-dimensional (2D) sheet. Although this aggregation model only describes growth in two dimensions (x and y), it is proposed that growth in the third dimension (z) simply results from the stacking of a number of these 2D sheets on top of each other, which would be hydrophobically driven. A reflection observed in the powder diffractogram of **2**, corresponding to a repeating distance of 10−11 Å, is in good agreement with the thickness of such stacked layers.[32] A similar stacking of layers has been proposed for razor-blade-like aggregates formed by pyridinium-functionalized molecular clips in water[24] and more recently also for the aggregates formed by molecular clips with long aliphatic tails in the solid state.[33] The unique features of these rectangular aggregates are their finite size and high monodispersity. The

(31) In the case of the sample prepared at 20 °C, it appeared that short (e.g., 1 min) or long (e.g., 1 day) incubation times did not result in major changes in the size distribution diagram observed for the sample, which was preincubated for 30 min. Aggregates of **2** were also prepared at 5 °C, and their size distribution diagram showed a polydispersity similar to that of the aggregates prepared at 20 °C.

(32) X-ray powder diffraction on samples of **2** revealed only a single, very broad reflection, corresponding to a repeating distance of approximately 10−11 Å. The absence of clear *d*-spacings suggests that the aggregates are built up from molecular units that interact in a very diverse way or assemble in a variety of geometries. Since the complex is a racemic mixture of Λ and Δ enantiomers, and since in the head-to-tail self-association process one molecule of **2** has the possibility to choose between different bipyridine ligands of a neighboring molecule of **2** for binding in its cleft and, additionally, has the option to use each of its own bipyridines to hold another molecule of **2**, such a diversity in binding can be easily envisaged.

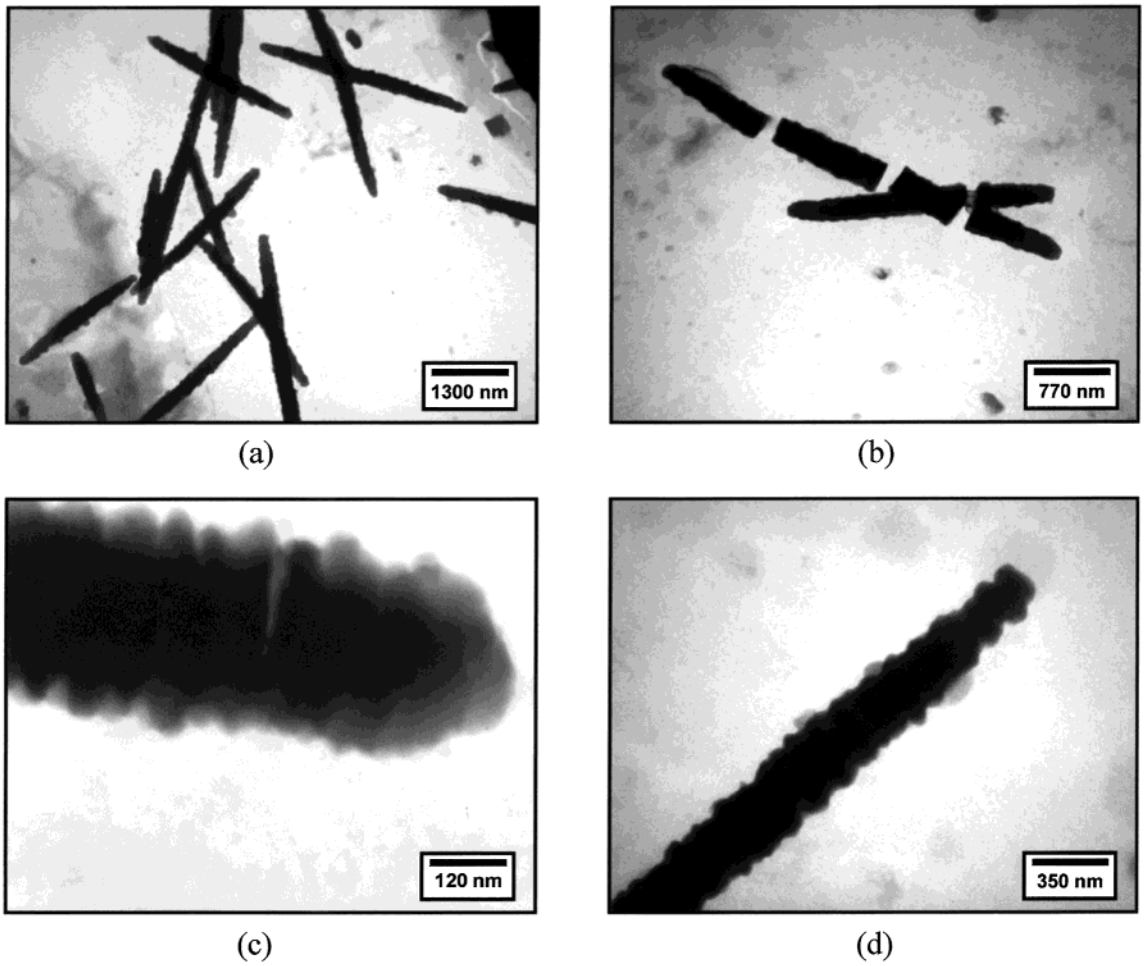

Figure 5. (a) TEM image of cigarlike aggregates formed by **2**. (b) TEM image of cigars displaying transverse cracks. (c, d) Magnifications of cigars, which show that they are built up from smaller subunits. Samples are not shadowed or stained.

fact that the aggregates are not infinite, as they are in the case of **1**, is attributed to several factors. First, following the proposed growth mechanism, it can be expected that in the center of the aggregate of **2** the interactions between the molecules are the strongest, both between the two partners of the dimer and between the naphthalene surfaces of neighboring dimers. In the regions of the aggregate containing the head-to-tail attached molecules, the aromatic surfaces of neighboring molecules of **2** are less overlapping. Hence, it is likely that the interactions between the molecules in the head-to-tail growing part are weaker than the interactions between the molecules in the center of the aggregate. As the aggregate grows, it can be expected that after a certain moment it will be energetically no longer favorable to attach new monomers to the relatively water-soluble exterior of the aggregates of **2**.[34] At this point, the assembly stops growing. The final shape of the architecture is thus governed by a subtle balance between the enthalpy (strength of intermolecular interactions) and the entropy of the self-assembly process. It should be further noted that even at higher concentrations of **2** (e.g., 2% w/v), larger aggregates are not observed, suggesting that the thermodynamic equilibrium controls the final structure. Finally, it cannot be excluded that the stereochemistry of the monomer building blocks of **1** and **2** plays a role in the final shape of the aggregates. It is possible that the aggregates consist of only enantiomerically pure molecules, racemic mixtures, or conglomerates. Obviously, as a result of this, the interactions between the molecules within the resulting aggregate structures can differ significantly.[35] Future research will therefore be focused on separation of the enantiomers of **1** and **2** and on the study of their respective aggregation behavior.

In the proposed model, the edges of the aromatic side walls of the receptor part of **2** form the floor and the roof of the rectangles. Compared to the ruthenium−bipyridine groups at the edges of the rectangles, these sides are hydrophobic. This might be the reason that the rectangles in some cases organize themselves further, tilted on their edges, into a cigarlike superstructure, in which all the relatively hydrophobic rectangular faces minimize their exposure to water (Figure 7). Similar hierarchical growth processes have been observed in natural[36] as well as in artificial systems.[37]

The electron microscopic studies revealed that at high temperature the size of the rectangular aggregates becomes

(33) (a) Holder, S. J.; Elemans, J. A. A. W.; Barberá, J.; Rowan, A. E.; Nolte, R. J. M. *Chem. Commun.* **2000**, 353. (b) Holder, S. J.; Elemans, J. A. A. W.; Donners, J. J. J. M.; Boerakker, M. J.; de Gelder, R.; Barberá, J.; Rowan, A. E.; Nolte, R. J. M. *J. Org. Chem.* **2001**, *66*, 391.

(34) This is reflected in the short aggregation width of the rectangular aggregates (2 × 75 nm, corresponding to approximately 2 × 40 molecules of **2**).

(35) (a) Kitaigorodskii, A. I. In *Molecular Crystals and Molecules*; Academic Press: New York, 1973. (b) Breu, J.; Domel, H.; Stoll, A. *Eur. J. Inorg. Chem.* **2000**, 2401, and references therein.

(36) Tsai, C. J.; Ma, B. Y.; Kumar, S.; Wolfson, H.; Nussinov, R. *Crit. Rev. Biochem. Mol.* **2001**, *36*, 399.

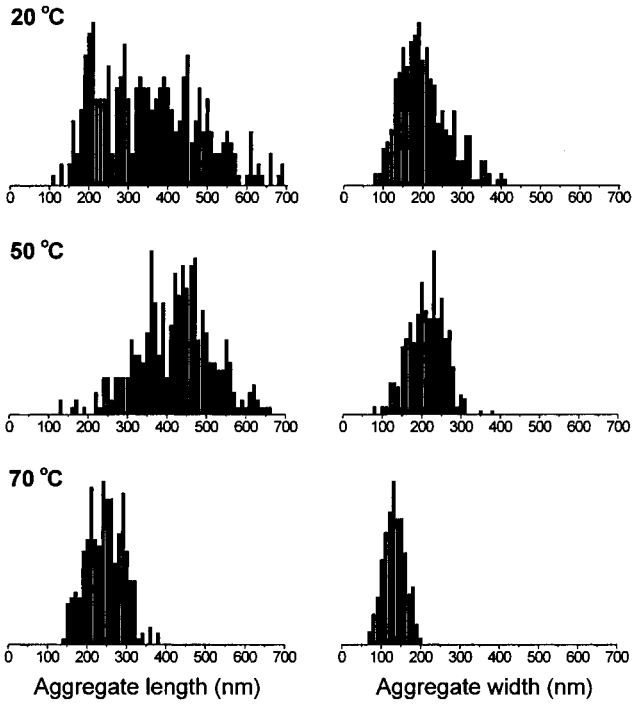

Figure 6. Size distribution diagrams of lengths and widths of rectangular aggregates formed by **2** at various temperatures (each diagram contains 300−400 data points).

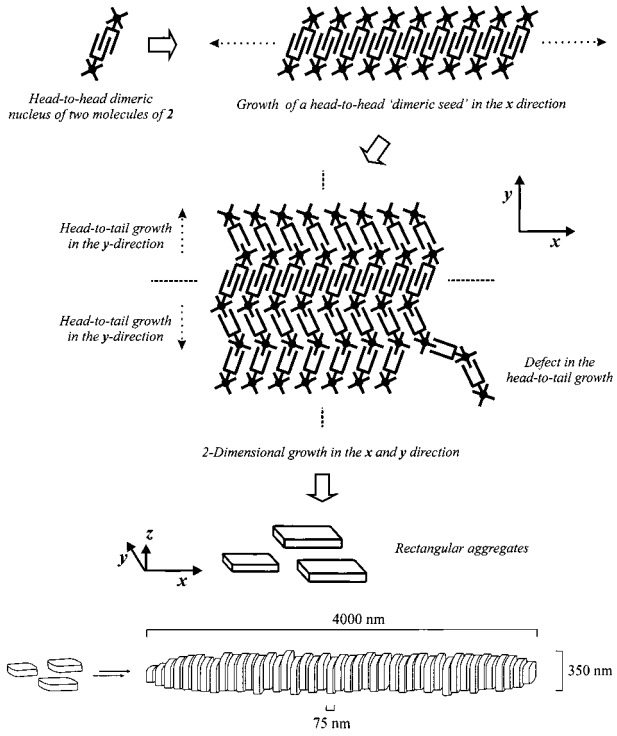

Figure 7. Proposed aggregate growth of **2**.

smaller and more monodisperse. The first effect was expected and can be explained by the fact that the strength of the interactions between the molecules of **2**, and consequently the aggregate size, decreases at higher temperature. The unexpected higher monodispersity is proposed to be the result of a self-repair process analogous to the repair processes observed in natural systems.[38] The chiral nature of the molecules of **2** can result in several packing geometries, all of different energies. At higher temperatures, as a result of the increased kinetics, only the most favorable aggregation modes occur and hence a more defined structure is obtained. Self-association that occurs via the most optimum assembly geometry eventually leads to the most stable structure. Those monomers of **2** that assemble in a geometry with relatively weak interactions fall off more easily at higher temperatures before further growth occurs.

Conclusions

New water-soluble metallohosts, viz., ruthenium−bipyridine centers functionalized with a receptor cavity, have been synthesized. The amphiphiles with a benzene side-walled cavity appear to self-associate in water to form well-defined dimers, which further self-assemble to generate undefined mesoscopic assemblies. Enlargement of the receptor side walls, viz., with naphthalene moieties, increases the interaction between the molecules, and as a result discrete rectangular aggregates and cigarlike objects are formed. The rectangular assemblies are very monodisperse in shape and also relatively monodisperse in size. At higher temperatures, smaller rectangular architectures are formed with an even greater monodispersity in size. The organization of the molecules into rectangular and higher cigarlike aggregates is a unique example of a hierarchical growth self-assembly process.

The present work shows that, to obtain well-defined nanosized architectures, sufficiently strong interactions between the constituting amphiphiles are needed. A combination of strong head-to-head and head-to-tail growth processes is required to achieve the discrete nanosized architecture. Future work will be focused on obtaining control over the subtle balance between the enthalpy and entropy factors of the growth process, on control over the size and shape of the nanostructures, and on the exact mechanism of the hierarchical self-assembly of the rectangular aggregates into the cigars.

Experimental Section

Materials and General Methods. DMF was dried over BaO for 1 week and then vacuum-distilled; the first 30% of the distillate was removed. Diethyl ether was distilled under nitrogen from sodium benzophenone ketyl. All other chemicals were commercial products and were used as received. For column chromatography, neutral alumina purchased from Aldrich was dried overnight in an oven at 150 °C, and then 6% (w/w) water was added and the mixture was equilibrated by rotation in a round-bottom flask on a closed rotary evaporator for 3 h.

NMR Experiments. ^{1}H NMR dilution titrations in D_2O were carried out in the presence of an external standard (trimethyl phosphate in D_2O, $\delta = 0.00$ ppm). Two-dimensional NOESY spectra were recorded by applying a mixing time of 750 ms. Self-association constants were determined in duplicate by recording the NMR spectra of at least 10 samples containing different concentrations of the host molecule. These concentrations varied from the minimum concentration needed for detection with ^{1}H NMR (∼0.2 mM) to approximately 10 mM or the maximum solubility of the compound. The shifts of the probe protons

(37) See, for example: (a) Jenekhe, S. A.; Chen, X. L. *Science* **1999**, *283*, 372. (b) Li, M.; Schnablegger, H.; Mann, S. *Nature* **1999**, *402*, 393. (c) Choi, I. S.; Bowden, N.; Whitesides, G. M. *Angew. Chem., Int. Ed.* **1999**, *38*, 3079. (d) Berl, V.; Huc, I.; Lehn, J.-M.; Schmutz, M. *Chem. Eur. J.* **2000**, *6*, 1938. (e) Brunsveld, L.; Zhang, H.; Glasbeek, M.; Vekemans, J. A. J. M.; Meijer, E. W. *J. Am. Chem. Soc.* **2000**, *122*, 6175.
(38) Modrich, P. *Annu. Rev. Biochem.* **1987**, *56*, 435.

(in hertz) were plotted versus concentration (in moles per liter), and the obtained titration curves were fitted to eq 1, which defines a 1:1 self-association of two molecules:

$$\delta_{obs} = \delta_m + \frac{(\delta_m + \delta_d)(1 + 4cK_{self} - \sqrt{1 + 8cK_{self}})}{4cK_{self}} \qquad (1)$$

In eq 1 δ_{obs} and c are the observed shift (in hertz) and the concentration (in moles per liter), respectively. From the fitting procedure, the self-association constant K_{self} and the CIS value ($\delta_d - \delta_m$ = calculated shift of the dimer minus the calculated shift of the monomer) can be obtained.

Molecular Modeling Studies. Molecular modeling calculations were performed on a Silicon Graphics Indigo II workstation by use of the Quanta package with the CHARMm 3.3 force field.[39] All calculations were carried out in a vacuum, with ABNR minimization. The dimeric structures of **1** and **2** were calculated with the nOe contacts observed by NMR, incorporated in the calculation by use of the nOe constraints option within the Quanta CHARMm package.

Fluorescence Measurements. Fluorescence spectra were recorded on a Perkin-Elmer luminescence spectrometer LS50B equipped with a thermostated cuvette holder (T = 25 °C). Samples of various concentrations of compounds **1** and **2** and $[Ru(bipy)_3]Cl_2$ in demineralized water in a 1.00 cm, 4 mL quartz cuvette were purged with argon to exclude fluorescence quenching by oxygen. The excitation wavelength was the wavelength of the MLCT band observed in the UV−vis spectra of the compounds. The excitation and emission slits were 15 nm. The emission spectra were recorded from 500 to 750 nm at a scanning speed of 120 nm min^{-1}.

Electron Microscopy Studies. A drop of a sample of **1** or **2** in demineralized water was deposited on a Formvar-coated copper grid. After 45 s, the excess dispersion was removed. The grids were studied on a Philips TEM 201 instrument operating at 60 kV. In some cases, the grids were shadowed with platinum (under an angle of 45°, layer thickness 2 nm). For the variable temperature TEM experiments, which were carried out in duplicate, samples of **2** having identical concentrations in demineralized water were prepared and then heated to the desired temperature in a water bath. After equilibration for 30 min, a drop of the sample was deposited on a grid and studied as described above. Size distribution diagrams were obtained by measuring the lengths and widths of 300−400 aggregates.

Powder Diffraction Studies. A drop of a 5 mM sample of **1** or **2** in D_2O was placed on a silicon single crystal, which was then placed in a desiccator containing fresh P_2O_5 as drying agent. The sample was stored in vacuo for 24 h, and then placed in a Philips PW1710 diffractometer, which was equipped with a Cu LFF X-ray tube operating at 40 kV and 55 mA [wavelengths (α1, α2): 1.54060, 1.54438].

Syntheses: Compound 3. 5,6-Dihydro[1,10]phenanthroline-5,6-dione[22] (1.0 g, 4.8 mmol) and urea (580 mg, 9.7 mmol) were suspended in toluene (20 mL). Trifluoroacetic acid (1.5 mL) was added and the mixture was refluxed under nitrogen for 16 h with use of a Dean and Stark trap. After cooling, the brown lumps were filtered off and suspended in ethanol (20 mL), and the mixture was refluxed for 1 h. After cooling, the yellow precipitate was filtered off, washed with ethanol (50 mL) and diethyl ether (50 mL), and dried under vacuum to yield 1.2 g of 3 (86%) as a pale yellow solid.

Mp > 400 °C (decomp); IR (KBr pellet) ν = 3174 (NH), 1737, 1707, 1689 (C═O), 1481, 1459, 1430 (C═C, C═N), 1143, 1122, 1063, 959 (ArH) cm^{-1}; ^{1}H NMR (DMSO-d_6, 300.14 MHz) δ = 8.72 (dd, 2H, bipy*H*-6, ^4J = 1.5 Hz, ^3J = 4.5 Hz), 8.35 (s, 4H, N*H*), 8.13 (dd, 2H, bipy*H*-4, ^4J = 1.5 Hz, ^3J = 7.2 Hz), 7.60 (dd, 2H, bipy*H*-5, ^3J = 4.5 Hz, ^3J = 7.2 Hz) ppm; ^{13}C{^{1}H} NMR (DMSO-d_6, 75.47 MHz) δ = 163.5 (urea *C*═O), 154.2 (bipyC-6), 148.8 (bipyC-2), 139.3 (bipy*C*-4) 135.1 (bipy*C*-3), 128.8 (bipy*C*-5), 77.8 [N*C*(Ar)N] ppm; MS (FAB) *m*/*z* 295 $[M + H]^+$. Anal. Calcd for $C_{14}H_{10}N_6O_2(0.5C_2H_6O)$: C, 56.78; H, 4.13; N, 26.49. Found: C, 56.93; H, 3.73; N, 26.75.

Compound 4. DMSO (10 mL) was purged with argon for 30 min. Powdered KOH (300 mg, 5.3 mmol) was added and the mixture was stirred for another 15 min. Compound **3** (300 mg, 1.0 mmol) and 1,2-bis(bromomethyl)benzene (540 mg, 2.0 mmol) were added while the mixture was cooled in a water bath (15 °C). The mixture was stirred for 16 h and then poured into a saturated aqueous NaCl solution (150 mL). The product was extracted with CH_2Cl_2 (2 × 100 mL), and the combined organic layers were washed with a saturated aqueous NaCl solution (150 mL) and water (150 mL) and then dried ($MgSO_4$). After filtration, the crude product was recrystallized from methanol (6 mL) to give 160 mg (31%) of **4** as a pale yellow solid. Single crystals of **4** were obtained by slow diffusion of methanol in a solution of the compound in chloroform.

Mp 354−355 °C (decomp); IR (KBr pellet) ν = 3111, 3056 (ArH), 2925, 2853 (CH_2), 1716 (C═O), 1579, 1568, 1461, 1428 (C═C, C═N), 1301, 1282, 1270 (CH_2), 1145, 923, 761 (ArH) cm^{-1}; ^{1}H NMR ($CDCl_3$, 300.13 MHz) δ = 8.92 (dd, 2H, bipy*H*-6, ^3J = 4.6 Hz, ^4J = 1.5 Hz), 7.89 (dd, 2H, bipy*H*-4, ^3J = 8.2 Hz, ^4J = 1.5 Hz), 7.32 (dd, 2H, bipy*H*-5, ^3J = 8.2 Hz, ^3J = 4.6 Hz), 7.29 (br s, 8H, Ar*H* side wall), 4.98 (d, 4H, NC*H*$_2$Ar *in*, ^2J = 16.7 Hz), 4.70 (4H, NC*H*$_2$Ar *out*, ^2J = 16.7 Hz) ppm; ^{13}C{^{1}H} NMR ($CDCl_3$, 75.47 MHz) δ = 158.53 (urea *C*═O), 151.44 (bipy*C*-6), 147.57 bipy*C*-2), 136.27 (bipy*C*-4), 135.38 (bipy*C*-3), 129.98 (Ar*C para* to CH_2N), 128.06 (Ar*C ortho* to CH_2N), 127.39 (Ar*C ipso* to CH_2N), 123.73 (bipy*C*-5), 77.42 [N*C*(Ar)N], 46.25 (N*C*H$_2$Ar) ppm; MS (FAB) *m*/*z* 499 $[M + H]^+$. Anal. Calcd for $C_{30}H_{22}N_6O_2(CH_4O)$: C, 70.18; H, 4.94; N, 15.83. Found: C, 70.41; H, 5.11; N, 15.44.

Compound 5. Starting from **3** (250 mg, 0.850 mmol) and 2,3-bis-(bromomethyl)naphthalene[40] (535 mg, 1.70 mmol), in DMSO (15 mL) with powdered KOH (260 mg, 4.63 mmol), this compound was synthesized as described for **4.** Yield 130 mg (26%) of **5** as a pale yellow solid.

Mp > 400 °C (decomp); IR (KBr pellet) ν = 3097, 3060 (ArH), 2956, 2923 (CH_2), 1713 (C═O), 1570, 1565, 1457, 1425, 1407 (C═C, C═N), 1327, 1278 (CH_2), 1125, 937, 789, 746 (ArH) cm^{-1}; ^{1}H NMR (300.13 MHz, $CDCl_3$) δ = 8.96 (dd, 2H, bipy*H*-6, ^3J = 4.6 Hz, ^4J = 1.5 Hz), 8.16 (dd, 2H, bipy*H*-4, ^3J = 8.1 Hz, ^4J = 1.5 Hz), 7.76 (s, 4H, naph*tH*-1,4), 7.76−7.70 (m, 4H, naph*tH*-5,8), 7.48−7.42 (m, 4H, naph*tH*-6,7), 7.36 (dd, 2H, bipy*H*-5, ^3J = 8.1 Hz, ^3J = 4.6 Hz), 5.10 (d, 4H, NC*H*$_2$Ar *in*, ^2J = 16.7 Hz), 4.92 (d, 4H, NC*H*$_2$Ar *out*, ^2J = 16.7 Hz) ppm; ^{13}C{^{1}H} NMR ($CDCl_3$, 75.47 MHz) δ = 158.30 (urea *C*═O), 151.55 (bipy*C*-6), 147.71 (bipy*C*-2), 136.02 (bipy*C*-4), 133.07 (naph*tC para* to CH_2N), 132.44 (naph*tC ipso* to CH_2N), 129.35 (naph*tC*-1,4), 128.23 (bipy*C*-3), 127.56 (naph*tC*-5,8), 126.63 (naph*tC*-6,7), 123.85 (bipy*C*-5), 79.20 [N*C*(Ar)N], 46.66 (N*C*H$_2$Ar) ppm; MS (FAB) *m*/*z* = 599 $[M + H]^+$. Anal. Calcd for $C_{28}H_{26}N_6O_2(CH_2Cl_2)$: C, 68.52; H, 4.13; N, 12.36. Found: C, 68.86; H, 4.10; N, 12.05.

Metallohost 1. A degassed solution of **4** (100 mg, 0.201 mmol) and $[Ru(bipy)_2]Cl_2 \cdot 2H_2O$[23] (105 mg, 0.202 mmol) in DMF (15 mL) was stirred under nitrogen at 110 °C for 16 h. After cooling, diethyl ether (100 mL) was added while the mixture was stirred vigorously. The purple precipitate was filtered off. The product was purified by column chromatography (alumina act. III, gradient elution, CH_2Cl_2 to CH_2Cl_2/MeOH, 97:3 v/v). The purified compound was dissolved in a minimal amount of methanol, and the resulting solution was added dropwise to stirred diethyl ether. After filtration of the resulting product, 108 mg (55%) of **1** was obtained as an orange-red hygroscopic solid, which was stored under nitrogen at −18 °C.

Mp > 400 °C (decomp); IR (KBr pellet) ν = 3052, 3017 (ArH), 2978 (CH_2), 1725, 1708 (C═O), 1464, 1445, 1430 (C═C, C═N), 1299, 1272, 1246 (CH_2) cm^{-1}; ^{1}H NMR (D_2O, 30 mM, 500.13 MHz) δ = 8.92 (d, 2H, bipy*H*−*d*, ^3J = 8.0 Hz), 8.55 (d, 2H, bipy*H*-3′, ^3J = 8.0

(39) CHARMm verison 22.0, Revision 920911; Resident and Fellows of Harvard College, 1984, 1992, with the use of template charges.

(40) Sisti, A. J.; Meyers, M. *J. Org. Chem.* **1973**, *38*, 4431.

Hz), 8.49 (d, 2H, bipy*H-3*, ^3J = 8.0 Hz), 8.18 (d, 2H, bipy*H-f*, ^3J = 5.5 Hz), 8.09 (td, 2H, bipy*H-4′*, ^3J = 8.0 Hz, ^4J = 1.5 Hz), 7.81 (td, 2H, bipy*H-4*, ^3J = 8.0 Hz, ^4J = 1.5 Hz), 7.77 (d, 2H, bipy*H-6*, ^3J = 5.5 Hz), 7.73 (d, 2H, bipy*H-6′*, ^3J = 5.5 Hz), 7.61 (dd, 2H, bipy*H-e*, ^3J = 8.5 Hz, ^3J = 5.5 Hz), 7.43 (td, 2H, bipy*H-5′*, ^3J = 8.0 Hz, ^4J = 1.5 Hz), 7.03−6.96 (m, 4H, Ar*H-a* side wall), 6.87−6.79 (m, 4H, Ar*H-b* side wall), 6.75 (td, 2H, bipy*H-5*, ^3J = 8.0 Hz, ^4J = 1.5 Hz), 5.05 (d, 2H, NCH_2-*c′*Ar *in*, ^2J = 17.0 Hz), 4.93 (d, 2H, NCH_2-*c*Ar *in*, ^2J = 17.0 Hz), 4.50 (d, 2H, NCH_2-*c′*Ar *out*, ^2J = 17.0 Hz), 4.42 (d, 2H, NCH_2-*c*Ar *out*, ^2J = 17.0 Hz) ppm (for the proton numbering see the drawing of the molecule in Chart 1); $^{13}C\{^1H\}$ NMR (CD_3OD, 75.47 MHz) δ = 159.12, 158.91 (both urea *C*═O), 154.07, 153.42, 153.05, 152.12, 140.13, 138.20, 137.84, 134.54, 131.99, 131.54, 129.94, 129.66, 129.56, 129.44, 129.39, 126.30 (all Ar*C*), 79.91 [N*C*(Ar)N], 47.77, 47.42 (both N*C*H_2Ar) ppm; UV−vis (H_2O) λ/nm, log (ϵ/M^{-1} cm^{-1}) 283 (4.70), 447 (3.99); MS (FAB) *m*/*z* 912 $[M - 2Cl]^+$. HRMS (FAB) calcd for $[C_{50}H_{38}N_{10}O_2Ru]^{2+}$: 912.2228. Found: 912.2236.

Metallohost 2. Starting from **5** (46 mg, 0.077 mmol) and $[Ru(bipy)_2]Cl_2 \cdot 2H_2O$[23] (40 mg, 0.077 mmol) in DMF (6 mL), this compound was synthesized as described for **1**. Yield 72 mg (87%) of **2** as an orange-red hygroscopic solid, which was stored under nitrogen at −18 °C.

Mp > 400 °C (decomp); IR (KBr pellet) ν = 3050, 3012 (ArH), 2980 (CH_2), 1725, 1707 (C═O), 1467, 1444, 1434 (C═C, C═N), 1298, 1270, 1243 (CH_2) cm^{-1}; ^1H NMR (D_2O, 2 mM, 500.14 MHz) δ 9.12 (br d, 2H, bipy*H-d*, ^3J = 6.9 Hz), 8.44 (br d, 2H, bipy*H-f*, ^3J = 4.7 Hz), 8.32 (br m, 4H, bipy*H-3* and bipy*H-3′*), 8.00 (br m, 2H, bipy*H-4′*), 7.88 (br m, 2H, bipy*H-4*), 7.78 (br m, 2H, bipy*H-e*), 7.64 (br m, 4H, bipy*H-6′* and bipy*H-6*), 7.39 (br m, 4H, bipy*H-5′* and Ar*H-b′* side wall), 7.29 (br m, 2H, Ar*H-b′* side-wall), 7.20 (br m, 2H, bipy*H*), 6.97 (br m, 4H, Ar*H-b* side wall), 5.68 (br m, 4H, Ar*H-a* side-wall), 5.20 (d, 2H, NCH_2Ar *in*, ^2J = 16.5 Hz), 5.09 (d, 2H, NCH_2Ar *in*, ^2J = 16.5 Hz), 4.60 (d, 2H, NCH_2-*c′*Ar *out*, ^2J = 16.5 Hz), 4.47(d, 2H, NCH_2-*c*Ar *out*, ^2J = 16.5 Hz) ppm (for the proton numbering see the drawing of the molecule in Chart 1); $^{13}C\{^1H\}$ NMR (CD_3OD, 75.47 MHz) δ = 150.70, 158.31 (both urea *C*═O), 154.08, 153.63, 152.59, 152.42, 140.02, 139.34, 137.86, 135.50, 134.57, 133.88, 130.77, 130.25, 129.92, 129.46, 128.85, 128.14, 126.13, 125.90 (all Ar*C*), 79.23 [N*C*(Ar)N], 47.71, 47.51 (both N*C*H_2Ar) ppm; UV−vis (H_2O) λ/nm, log (ϵ/M^{-1} cm^{-1}) 284 (4.62), 450 (3.89); MS (FAB) *m*/*z* 1011 $(M - 2Cl)^+$. HRMS (FAB) calcd for $[C_{58}H_{42}N_{10}O_2Ru]^{2+}$: 1012.254. Found: 1012.209.

Supporting Information Available: ^1H NMR spectra of **1** and **2** in water, NMR dilution titration curves of **1**, fluorescence dilution titration curves of the ruthenium complexes, and the X-ray powder diffraction spectrum of **2**. This material is available free of charge on the Internet at http://www.pubs.acs.org.

JA012061I